Photoinduced coherent magnetization precession in epitaxial $La_{0.67}Ca_{0.33}MnO_3$ films

D. Talbayev,* H. Zhao, and G. Lüpke
Department of Applied Science, The College of William and Mary, Williamsburg, Virginia 23187-8795, USA

A. Venimadhav and Qi Li
Department of Physics, Pennsylvania State University, University Park, Pennsylvania 16802-6300, USA
(Received 22 August 2005; revised manuscript received 29 November 2005; published 19 January 2006)

Optically excited uniform magnetization precession in the ferromagnetic state of $La_{0.67}Ca_{0.33}MnO_3$ films grown on different substrates is investigated by the time-resolved magneto-optic Kerr effect. The parameters of magnetic anisotropy are determined from the measured field dependence of the precession frequency. The dominant anisotropy contribution in the film grown on $SrTiO_3$ (001) is the strain-induced easy-plane anisotropy. In the strain-free films on $NdGaO_3$ (110), we discover a uniaxial in-plane anisotropy that results from the interface due to the tilting of the oxygen octahedra in $NdGaO_3$.

DOI: 10.1103/PhysRevB.73.014417 PACS number(s): 76.50.+g, 75.30.Gw, 75.47.Lx, 75.70.Ak

I. INTRODUCTION

Half-metallic nature[1] of manganites makes them technologically important materials for magnetic tunnel junctions[2–4] and spin injection structures.[5,6] The understanding of the magnetization dynamics in manganite thin films is important for the fastest switching operation of these devices. Several factors, such as the possible normal modes and the damping of the coherent magnetization precession, play a crucial role in achieving reliable switching behavior. In this paper, we investigate the dynamical magnetization response of $La_{0.67}Ca_{0.33}MnO_3$ (LCMO) thin films to an ultrashort laser pulse. LCMO belongs to a family of colossal magnetoresistance manganites and undergoes a transition to a ferromagnetic state at $T_C \approx 250$ K. Earlier investigations of magnetization dynamics in manganite thin films have been performed by ferromagnetic resonance (FMR) measurements, where the absorption of an alternating microwave field is measured as a function of a static magnetic field.[7–12] However, only subnanosecond or 100-picosecond dynamics with a fixed magnitude of the magnetization vector can be explored because of the low frequency (10 GHz) used in FMR and the direct coupling of the microwave field to the magnetization. On the long time scale accessible to FMR, the dynamics is governed entirely by the magnetic anisotropy of the film. The angular dependence of the resonance field in the FMR experiment provides information on the anisotropy constants—parameters that are crucial for the design of thin-film devices. Most of the FMR studies, however, did not explore the magnetic anisotropy in detail, but focused on the magnetic homogeneity of the manganite films, which was evaluated from the FMR linewidth.

In ultrafast optical studies, the subpicosecond time resolution allows us to study the magnetic response that is much faster than the coherent precession of magnetization. A strong laser pulse first excites electrons in the sample. The sample's magnetic response is then monitored as a function of the time delay between the pump and probe pulses. The coupling of the laser-pulse excitation to the magnetization of the sample is not always readily understood, which underscores the importance of magneto-optic measurements. The high spatial resolution of the optical approach, compared to FMR, will prove useful in the study of microscopic magnetic elements.

The study of the picosecond magnetization dynamics of manganites was reported by Zhao *et al.*,[13] who monitored the optically induced conductance changes in LCMO films with 20-ps time resolution. Long-lived spin excitations were found responsible for a resistivity increase in the ferromagnetic phase. Several groups used time-resolved absorption measurements to study the photoinduced response of manganites. Matsuda *et al.*[14] reported that the gradual change (200 ps) in the photoinduced absorption reflects the photoinduced demagnetization (PID) in $(Nd_{0.5}Sm_{0.5})Sr_{0.4}MnO_3$. More detailed studies by Lobad and co-workers[15,16] and Averitt *et al.*[17] of LCMO attributed the ultrafast component (100 fs) of the photoinduced absorption to electron-lattice thermalization. The slower change in absorption (20–200 ps) was ascribed to the PID driven by the spin-lattice thermalization. A long-lived spin relaxation component was found in $Nd_{0.67}Sr_{0.33}MnO_3$ in transient reflectivity measurements by Ren *et al.*[18] The relaxation was shown to be magnetic in origin and dependent on the strain induced by different substrates. In these studies, slow changes in the optical absorption were interpreted as the magnetization response. Subsequent studies by Ogasawara *et al.*[19] and McGill *et al.*[20,21] employed the time-resolved magneto-optic Kerr effect (TR-MOKE) to study the magnetization dynamics. Ogasawara *et al.* found that after photoexcitation, the magnetization in $La_{0.6}Sr_{0.4}MnO_3$ (LSMO) decreases with a considerably longer time constant (1 ns) than the one measured by the transient absorption measurements.[14–17] McGill *et al.*[21] studied the magneto-optic response of LCMO near T_C and observed the PID together with an even slower Kerr transient which they attributed to photoinduced spin ordering.

Photoinduced demagnetization is not the only effect of a laser pulse impinging on a ferromagnetic sample. Ogasawara *et al.*[19] pointed out the presence of an oscillatory component in their TR-MOKE measurements, which they interpreted as a coherent precession of magnetization in LSMO. Photoin-

 ©2006 The American Physical Society

duced spin precession, to the best of our knowledge, was first reported by Ju *et al.*[22] in the study of optically excited exchange-biased NiFe/NiO bilayers. The precession of the NiFe magnetization was launched by the pump pulse via the "unpinning" of the exchange bias and detected by TR-MOKE. Optically induced magnetization precession was discovered, to the best of our knowledge in thin Ni films by Koopmans *et al.*,[23] who later confirmed[24] that the optically induced coherent precession and FMR are manifestations of the same phenomenon. They pointed out that the precession can be used as the "all-optical real-time ferromagnetic resonance" to study the properties of microscopic magnetic elements. Koopmans *et al.* argued that the coherent precession in their measurements was induced by the thermal modification of the anisotropy in the Ni film. Zhang *et al.*[25] induced the coherent magnetization precession in CrO_2 thin films by optically modulating the magnetic anisotropy of the films by nonthermal hot-electron spins. The work of Koopmans *et al.* and Zhang *et al.* demonstrated that the coherent precession in optical measurements is governed by the magnetic properties of the sample. Very recently, Zhao *et al.*[26] observed the photoinduced coherent precession in ultrathin Fe films on $Al_xGa_{1-x}As$ (001). A detailed study of the magnetic field and direction dependence of the precession frequency allowed them to fully characterize the in-plane magnetic anisotropy of the Fe films.

We report here on the photoinduced magnetization dynamics in LCMO thin films by TR-MOKE. We examine the field dependence of the precession frequency with the goal to determine the anisotropy of LCMO films grown on different substrates. FMR measurements could provide the same information. However, the absence of published FMR data, especially the in-plane orientational study of LCMO films grown on $SrTiO_3$ (001) (STO) and $NdGaO_3$ (110) (NGO), warrants the analysis presented in this paper. The precession excitation and relaxation mechanisms will be the subject of a separate publication.

Substrate-induced magnetic anisotropy has been attributed to a magnetoelastic interaction.[27–31] Static magnetization and FMR measurements on LSMO films by Kwon *et al.*[32] revealed a magnetic anisotropy that depends on the strain state of the film. Easy plane anisotropy was found in tensile-strained LSMO/STO films, and the easy normal-to-plane axis was discovered in compressively strained LSMO films grown on $LaAlO_3$ (001) (LAO). No in-plane anisotropy was detected by FMR. Similar magnetic anisotropy behavior was found in $Pr_{0.67}Sr_{0.33}MnO_3$ (PSMO) films by Wang *et al.*[33] PSMO films grown on STO and LAO displayed easy-plane and normal-to-plane easy-axis anisotropy, respectively. The anisotropy of the PSMO/NGO film could not be determined from magnetization measurements due to the large paramagnetic contribution of NGO. Suzuki *et al.*[27] and Steenbeck and Hiergeist[28] studied the anisotropy of strained LSMO films and reported an in-plane biaxial anisotropy. The two studies disagreed whether the [100] (Mn-O bond direction) or the [110] axes are the easy axes in the tensile-strained LSMO/STO films. O'Donnel *et al.*[29] found an easy plane and a biaxial in-plane anisotropy with [100] easy axes in LCMO/STO. Recent measurements by Xiong *et al.*[31] of magnetic anisotropy in LCMO films confirmed the dependence of the out-of-plane anisotropy constant on the amount of strain in the film, but revealed no in-plane anisotropy.

According to our analysis of the coherent precession in LCMO, the dominant anisotropy components are uniaxial normal-to-plane and uniaxial in-plane. The substrate-induced tensile strain in LCMO/STO films results in a strong magnetoelastic easy-plane anisotropy (H_a=0.7 T) and a considerably weaker anisotropy of tetragonal symmetry. The strain in the LCMO/NGO films is essentially zero due to a small lattice mismatch. The (110) face of the orthorhombic NGO substrate corresponds to the (001) face in the pseudocubic notation, which in combination with a negligible orthorhombic distortion should lead to magnetic anisotropy that has tetragonal symmetry, as in the LCMO/STO film. Unexpectedly, our measurements have revealed a strong in-plane uniaxial anisotropy in the LCMO/NGO films with the anisotropy field as large as H_u=0.3 T in the 100-nm-thick film. The in-plane easy axis is along the [110] direction in the pseudocubic unit cell, at 45° to the Mn-O bonds. The near-zero strain in the films leads to the conclusion that the uniaxial in-plane anisotropy is not strain-induced.

The paper is organized as follows: Sec. II describes the experimental method used to obtain the TR-MOKE spectra. Analysis of the data is presented in Sec. III, where we compare the field dependence of the precession frequency with theoretical fits and deduce the parameters of magnetic anisotropy. Section IV summarizes our results and concludes the paper. In the Appendix we provide the expressions used to calculate the uniform precession frequencies.

II. EXPERIMENT

The LCMO films were epitaxially grown by pulsed-laser deposition on two substrates—$SrTiO_3$ (100) and $NdGaO_3$ (110).[34,35] The film thicknesses are 60, 100, and 150 nm. The STO substrate induces biaxial tensile strain in LCMO films, while the NGO substrate induces very little strain.

We investigate the temporal evolution of the photoinduced precession in LCMO films by TR-MOKE. Van Kampen *et al.*[24] introduced the femtosecond laser pulses as both excitation and probe of spin waves in metallic ferromagnetic films. In our measurements, we use a 150-fs, 800-nm pump pulse from a Ti:sapphire amplifier system to induce the magnetization precession in the LCMO films. Most measurements are performed with the applied pump fluence of 5 mJ/cm^2. The fluences as low as 1 mJ/cm^2 and as high as 10 mJ/cm^2 do not change the overall appearance of the TR-MOKE spectra. The extracted precession frequency shows no dependence on the excitation power. To study the field dependence of the precession frequency, we mount the samples in the center of a split-coil superconducting magnet that allows optical access to the sample with the magnetic field being either in the film plane or almost normal to it. The variable-temperature inset of the magnet is used to control the sample temperature in the 20–55 K range.

When the applied magnetic field H_0 is in the film plane [Fig. 1(a)], the equilibrium position of magnetization is also

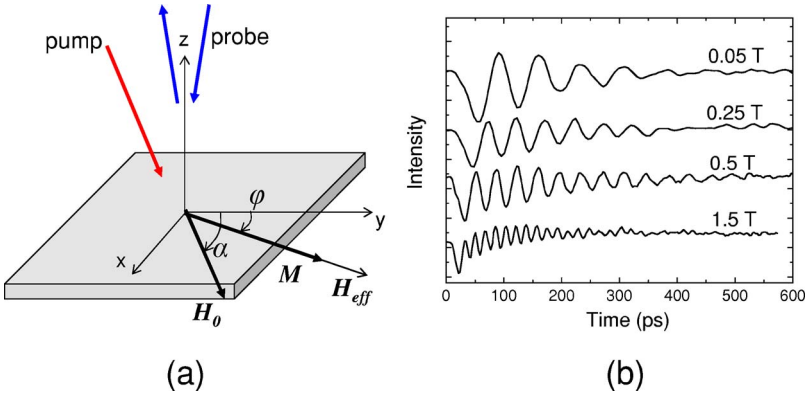

FIG. 1. (Color online) (a) Geometry of the pump-probe measurement with applied magnetic field. (b) Magnetization precession as measured by TR-MOKE in the 60-nm LCMO/NGO film at $T=20$ K and $\alpha=45°$, with α defined in (a).

in-plane along an equilibrium field H_{eff}, which is the sum of H_0 and the in-plane anisotropy fields. The incident pump pulse initiates the precession of the magnetization around its equilibrium direction along H_{eff} by inducing a transient field H_{tr}, possibly due to the instantaneous heating and lattice expansion[24] that changes the anisotropy of the film. The magnetization M starts to precess around H_{tr}, and when H_{tr} has vanished, the vector M starts to precess around H_{eff}. The time evolution of the precession is recorded by a delayed s-polarized probe pulse whose angle of incidence is close to zero [almost normal incidence, Fig. 1(a)]. In this polar geometry, the polarization rotation of the reflected probe pulse is proportional to the normal component of magnetization, M_z. We measure the precession by analyzing the polarization state of the reflected probe pulses and changing the time delay between pump and probe. Ogasawara *et al.*[19] have found that the Kerr rotation in LSMO is largest when the probe energy is about 3.1 eV, twice the energy of the pump. Therefore, we use a frequency-doubling crystal and 400-nm probe pulses to increase the sensitivity of our setup.

Figure 1(b) shows the precession of magnetization as recorded by TR-MOKE. The presented time-domain spectra clearly display the oscillatory variation of the light intensity that passes through the analyzer. Since the polarization rotation is proportional to the normal component of M, the frequency of the oscillation corresponds to the frequency of the magnetization precession. By performing a Fourier analysis of the time-domain spectra, we extract the field-dependent precession frequency. In the following section we present the measured frequency-field dependence and compare it with the established theory.

III. RESULTS AND DISCUSSION

A. LCMO/STO film

The field dependence of the precession frequency in the 100-nm thick LCMO/STO film is shown in Fig. 2. Panel (a) displays the frequencies measured with the in-plane field applied along two directions with an angle of 45° between them. The 0° measurement corresponds to the field applied along the [100] (Mn-O bond) direction. The different frequencies along the two field directions indicate that an in-plane magnetic anisotropy is present in the film.

The magnetization precession in ferromagnets is described by the torque equation

$$\dot{\boldsymbol{M}} = -\gamma \boldsymbol{M} \times \boldsymbol{H}_{\text{eff}}, \tag{1}$$

where $H_{\text{eff}i}=-\partial E/\partial M_i$, $i=x,y,z$, and E is the magnetic energy of the system. To explain the frequency-field dependence presented in Fig. 2, we need to introduce a uniaxial easy-plane anisotropy $K_a M_z^2/M_s^2$ ($K_a>0$) and a fourth-order tetragonal-symmetry anisotropy $-K_{\parallel}(M_x^4+M_y^4)/2M_s^4 - K_{\perp}M_z^4/2M_s^4$ with in-plane easy axes X and Y ($K_{\parallel}>0$) along the film's [100] and [010] directions. The magnetic part of the free energy can be written as

$$E = -\boldsymbol{H}_0 \cdot \boldsymbol{M} + 2\pi M_z^2 + K_a M_z^2/M_s^2 - K_{\parallel}(M_x^4 + M_y^4)/2M_s^4 - K_{\perp}M_z^4/2M_s^4, \tag{2}$$

where the first term represents the Zeeman energy and the second denotes the shape anisotropy energy due to demagnetization. The corresponding phenomenological fields are the demagnetizing field $H_d=4\pi M_s$ and the anisotropy fields

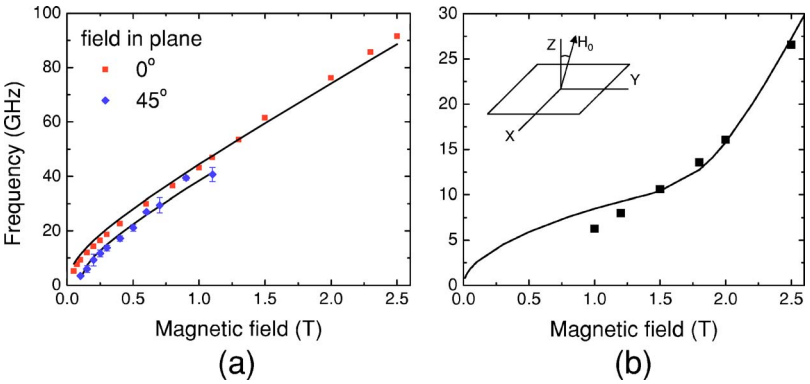

FIG. 2. (Color online) Field dependence of the precession frequency in LCMO/STO. Solid lines are calculated using the expressions given in the Appendix with effective fields given in Table I and a g factor of 1.98. (a) Applied magnetic field is in plane. The $\alpha=0°$ and $\alpha=45°$ orientations correspond to the field along the in-plane tetragonal easy axis and along the in-plane tetragonal hard axis, respectively. α is defined in Fig. 1. (b) Applied magnetic field is almost normal to the film and lies in the Y-Z plane, with Y being the tetragonal easy axis.

TABLE I. Anisotropy field values deduced from fits to the field dependence of the precession frequency in the LCMO/STO film.

Sample	H_d (T)	H_a (T)	$H_\perp$ (T)	$H_\parallel$ (T)
LCMO/STO	0.72	0.57+/−0.24	−0.30	0.031+/−0.054

$H_a=2K_a/M_s$, $H_\perp=2K_\perp/M_s$, and $H_\parallel=2K_\parallel/M_s$.

We have solved Eq. (1) for two special cases: when the applied field is in the plane of the film [Figs. 1(a) and 2(a)] and when the applied field is in the *Y*-*Z* plane [Fig.2(b)]. The expressions for resonance frequencies and magnetization equilibrium conditions can be found in the Appendix. We use the *g*-factor value of 1.98 in our analysis.[7] Solid lines in Fig. 2 show the calculated frequencies. In Fig. 2(a), the applied field is in the film plane and along the *Y* axis (or, equivalently, along the *X* axis) in the 0° measurement and at 45° to both *X* and *Y* axes in the 45° measurement. In Fig. 2(b), the applied field is in the *Y*-*Z* plane making a 4° angle with the sample normal. Each solid line represents a result of the least-square fitting procedure carried out separately for each set of data. Only two free parameters are used to fit the in-plane measurements in Fig. 2(a)—H_a and $H_\parallel$. We use the bulk magnetization value to calculate the demagnetization field $H_d=4\pi M_s=0.72$ T. To fit the out-of-plane measurement in Fig. 2(b), we use H_a, $H_\perp$, and $H_\parallel$ as fitting parameters. After fitting each measurement separately, we take the average values of the anisotropy fields and collect them in Table I.

The observed anisotropy constants are in good agreement with static magnetization studies of the effects of strain on the anisotropy in manganite films.[27,29–31] The dominant contribution is the uniaxial easy-plane anisotropy with $K_a=1.6\times10^5$ J/m^3, which is the same as measured by Ranno *et al.*[30] and O'Donnel *et al.*,[29] who found an easy-plane strain-induced anisotropy in tensile-strained LCMO/STO and LSMO/STO films. This uniaxial anisotropy constant K_a is larger than the one measured in the study of photoinduced precession in LSMO/STO.[36] The difference may result from the LCMO film being thinner than the LSMO film used in Ref. 19 and from LCMO being a lower-band-width manganite and, thus, being more susceptible to epitaxial strain. The perpendicular component of the tetragonal anisotropy $K_\perp=-0.86\times10^5$ J/M^3 agrees well with O'Donnel's fourth-order uniaxial easy-plane anisotropy constant. Our measurements also indicate the presence of an in-plane biaxial anisotropy ($K_\parallel=0.1\times10^5$ J/m^3) with its easy axes along the in-plane [100] and [010] directions, which corresponds to the directions of Mn-O bonds. Similar behavior was observed by O'Donnel *et al.* who measured a higher biaxial anisotropy constant due to their LCMO film being thinner than the critical thickness of 60 nm.[30] No in-plane anisotropy was found by Xiong *et al.*[31] in LCMO/STO films in 10–400-nm thickness range.

B. LCMO/NGO film

Figure 3 shows the field dependence of the precession frequency in a 100-nm-thick LCMO/NGO film with the applied field both in the plane of the sample and almost normal to it. The main difference from the frequencies measured in LCMO/STO is a finite frequency at fields as low as 0.01 T, which can be extrapolated to a finite precession frequency at zero field, although measurements at zero field are not always successful. The finite zero-field frequency in the out-of-plane measurement [Fig. 3(b)] can be explained by a large positive in-plane tetragonal anisotropy constant $K_\parallel$ in Eq. (2). The introduction of such a term leads to a pronounced fourfold symmetry in the in-plane magnetic properties. To verify that prediction, we study the frequency-field dependence as a function of the in-plane direction of the applied field [angle ϕ in Fig. 1(a)] and reveal a dominant twofold in-plane symmetry [Fig. 3(a)]. The field-dependent frequencies reach a maximum when we apply the magnetic field along a certain direction and a minimum upon rotation of the sample by 90°. The maximum-frequency direction corresponds to the 45° field angle and the minimum-frequency direction—to the 135° field angle in Fig. 3(a), representing the [110] and [1-10] crystallographic directions, respectively. The observed twofold symmetry requires the introduction of twofold sym-

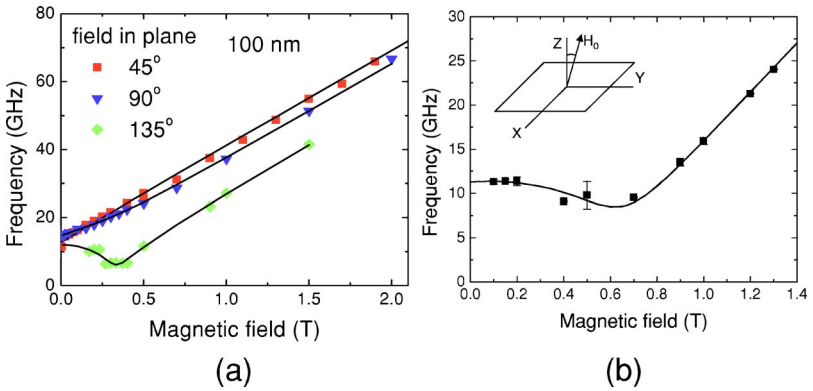

FIG. 3. (Color online) Field dependence of the precession frequency in LCMO/NGO, in the 100 nm* sample in Table II. Solid lines are calculated using the expressions given in the Appendix with effective fields given in Table II and a *g* factor of 1.98. (a) Applied magnetic field is in plane. The $\alpha=45°$, $\alpha=90°$, and $\alpha=135°$ orientations correspond to the field along the in-plane uniaxial easy axis, at 45° to the easy axis, and along the in-plane uniaxial hard axis, respectively. α is defined in Fig. 1. (b) Applied magnetic field is almost normal to the film and lies in the *Y*-*Z* plane, with *Y* being the uniaxial easy axis.

TABLE II. Anisotropy field values deduced from fits to the field dependence of the precession frequency in LCMO/NGO films. 100 nm* sample—measurements in Fig. 3. 60, 100, and 150 nm samples—measurements in Fig. 4.

Sample	H_d (T)	H_a (T)	$H_\perp$ (T)	$H_\parallel$ (T)	H_u (T)
100 nm*	0.72	−0.37+/−0.15	−0.08	0.003+/−0.006	0.31+/−0.01
60 nm	0.72	−0.17+/−0.25		0.01+/−0.06	0.20+/−0.10
100 nm	0.72	−0.25+/−0.21		−0.03+/−0.05	0.19+/−0.02
150 nm	0.72	−0.26+/−0.25		−0.03+/−0.04	0.09+/−0.07

metry terms in the magnetic free energy given by Eq. (2). The lowest-order anisotropy with required symmetry is an easy in-plane axis and has the form $-K_u M_{y'}^2/M_s^2$, where $M_{y'}$ is the component of the magnetization along the easy direction y'. We achieve the best agreement between the calculated frequencies and the measured ones when we choose the direction of y' to be along the maximum-frequency direction of Fig. 3(a) ([110] direction) and introduce a small biaxial anisotropy with easy axes along the [100] and [010] directions. According to Eq. (2), the X and Y directions in Fig. 1 are biaxial easy axes when $K_\parallel > 0$. Then the direction of y' is at 45° to both X and Y. The uniaxial in-plane anisotropy energy acquires the form $-K_u[M_x M_y + 1/2(M_x^2 + M_y^2)]/M_s^2$, and the total free energy reads

$$E = -\boldsymbol{H}_0 \cdot \boldsymbol{M} + 2\pi M_z^2 + K_a M_z^2/M_s^2 - K_\parallel (M_x^4 + M_y^4)/2M_s^4 - K_\perp M_z^4/2M_s^4 - K_u[M_x M_y + 1/2(M_x^2 + M_y^2)]/M_s^2. \quad (3)$$

We introduce the in-plane uniaxial anisotropy field as $H_u = 2K_u/M_s$.

The solution of the equation of motion with the free energy given by Eq. (3) for the two special cases shown in the left and the right panels of Fig. 3 can be found in the Appendix. Frequencies calculated using the described model are shown by solid lines in Fig. 3, and the parameters derived from least-square fits are given in Table II. These parameters are average values obtained from fitting the measurements with different orientations of the applied field for a single sample. The largest anisotropy terms in the 100-nm film are the easy normal-to-plane axis with $K_a \approx -1.1 \times 10^5$ J/m^3 and the easy in-plane axis at 45° to Mn-O bonds with $K_u = 0.9 \times 10^5$ J/m^3. The perpendicular easy-axis anisotropy has been previously observed in the study of magnetization dynamics in LSMO/NGO,[36] where it has been attributed to the uncertainty in the saturation magnetization that affects H_d and/or to the interface anisotropy. The perpendicular easy axis is not in contradiction with the symmetry of the film and the underlying substrate. The (110) plane of the orthorhombic NGO crystal corresponds to the (001) plane of the pseudocubic unit cell, and the LCMO film on (110) NGO grows in the (001) orientation due to the good match of the lattice parameters.[37]

The pseudocubic symmetry of LCMO and NGO and the lattice mismatch of only 0.1% between them suggest that the stress and the stress anisotropy are negligible. Therefore, the observed in-plane uniaxial anisotropy must be magnetocrystalline. To clarify the origin of the uniaxial anisotropy, we perform the TR-MOKE measurements on LCMO/NGO films of different thicknesses with magnetic field applied in the plane of the film. The recorded field dependence of the precession frequency for the films of 60, 100, and 150 nm thickness is shown in Fig. 4. The solid lines in the Figure show the calculated frequencies and Table II displays the deduced fitting parameters. The values in the table are averages over the measurements with different orientations of the applied field performed on the same sample. The twofold in-plane symmetry is clearly present in these samples, as evidenced by the different behavior of the precession frequency when the applied field is in the 45° orientation (along the easy axis)

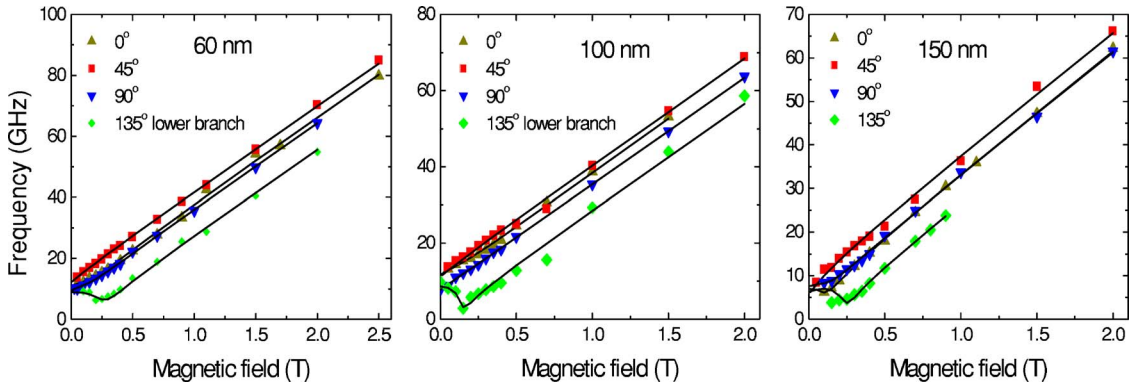

FIG. 4. (Color online) Field dependence of precession frequency in LCMO/NGO, in the 60, 100, and 150 nm samples in Table II. Solid lines are calculated using the expressions given in the Appendix with effective fields given in Table II and a g factor of 1.98. Applied magnetic field is in plane. In each panel the $\alpha = 45°$, $\alpha = 90°$, and $\alpha = 135°$ orientations correspond to the field along the in-plane uniaxial easy axis, at 45° to the easy axis, and along the in-plane uniaxial hard axis, respectively. α is defined in Fig. 1.

and in the 135° orientation (along the hard axis). The magnitude of the anisotropy field is almost the same in the 60-nm and 100-nm films and is diminished significantly in the 150-nm film. Despite the observed variation of the anisotropy field in the films of the same thickness (100 nm), we think that the trend of the decreasing anisotropy field with increasing film thickness is well established. A lower magnetic anisotropy in thicker films is well explained when the anisotropy is strain-induced. In our LCMO/NGO films the amount of strain is negligible. Therefore, we suggest that the lower anisotropy in the 150-nm film results from the interfacial origin of the anisotropy. If the surface energy density of the interface uniaxial anistropy is K_s, then the anisotropy enters the expression for the volume energy density as a term proportional to $K_u = K_s/d$, where d is the film thickness.[38] Thus, K_u is reduced in thicker films.

The in-plane uniaxial anisotropy in LCMO/NGO films was observed by Mathur *et al.*[39] in static magnetization measurements. Mathur *et al.* measured the anisotropy constant of 0.36×10^5 J/m^3 with the easy direction at 45° to Mn-O bonds, which coincides with the easy axis in our measurements. Mathur and collaborators argue that the anisotropy is substrate-induced and magnetocrystalline, although no specific anisotropy mechanism is described in their report. We believe that our and Mathur's observations document the same phenomenon. The crystallographic structure of NGO (Refs. 40 and 41) is orthorhombic with a $GdFeO_3$-type rotation of oxygen octahedra about the pseudocubic [111] direction. The rotation results in the modification of the pseudocubic (001) face of the substrate, causing the pseudocubic [110] diagonal to be different from the [1-10] diagonal. This could result in the described interface uniaxial anisotropy because oxygen environment of the Mn ions at the interface is different from that in the bulk. A similar magnetic anisotropy could be anticipated in LSMO/NGO films. Our previous study of the magnetization precession in LSMO (Ref. 36) does not give any evidence of a uniaxial in-plane anisotropy, although its presence cannot be ruled out because the precession with in-plane magnetic field has not been studied and the thickness of the studied films (160 nm) is higher than the thickness of the LCMO/NGO films.

IV. CONCLUSIONS

We have studied optically induced magnetization precession in thin LCMO films. The measured field dependence of the precession frequency is used to determine the parameters of magnetic anisotropy. In tensile-strained LCMO/STO films, the dominant contribution is the strain-induced easy-plane anisotropy—a property similar to that of the LSMO/STO films. In LCMO/NGO, our measurements reveal a strong in-plane uniaxial anisotropy with its easy direction at 45° to Mn-O bonds. We suggest that the anisotropy originates from the LCMO/NGO interface, where the MnO_6 octahedra are different from those in the bulk of the film. The modification of the oxygen octahedra results from the $GdFeO_3$-type oxygen octahedron rotation in NGO. The uniaxial anisotropy in the LCMO/NGO system must be taken into account in the fabrication of magnetic tunnel junctions.

ACKNOWLEDGMENTS

This work was supported in part by NSF (Contract Nos. DMR-0137322, IMR-0114124, and PSU MRSEC DMR-0213623), DOE (Grant No. DE-FG02-04ER46127), and the Petroleum Research Fund.

APPENDIX

We provide the solutions of Eqs. (1) and (3) for several special cases relevant to our study.

The measurement configuration with the in-plane magnetic field can be described by the angle of the applied field α and the equilibrium angle of magnetization ϕ (Fig. 1). The equilibrium position of magnetization is always in-plane and given by

$$H_0 \sin(\alpha - \phi) - \frac{H_\parallel}{4} \sin 4\phi + \frac{H_u}{2} \cos 2\phi = 0, \quad \text{(A1)}$$

where H_0 is the applied magnetic field, $H_\parallel$ and H_u are the in-plane tetragonal and in-plane uniaxial anisotropy fields. The precession frequencies are calculated to be

$$\omega = \gamma \sqrt{ab}, \quad \text{(A2)}$$

where a and b are given by

$$a = H_0 \cos(\alpha - \phi) + H_d + H_a + \frac{H_u}{2}(1 + \sin 2\phi) + H_\parallel(\sin^4\phi + \cos^4\phi), \quad \text{(A3)}$$

$$b = H_0 \cos(\alpha - \phi) + H_u \sin 2\phi + H_\parallel \cos 4\phi, \quad \text{(A4)}$$

where H_d is the demagnetization field, H_a is the uniaxial anisotropy field with its axis normal to the plane, and $H_\perp$ is the normal component of the tetragonal anisotropy field. To calculate the frequency for a certain field H_0 applied at an angle α, we first solve Eq. (A1) for the equilibrium position ϕ of magnetization and then use (A2)–(A4) to calculate the frequency. Solutions of Eq. (2) which describe the field-in-plane measurements on LCMO/STO are obtained from (A1), (A3), and (A4) by setting $H_u = 0$.

We now give the expressions for the precession frequency that describe the out-of-plane measurements on LCMO/STO shown in Fig. 2(b). The applied field is assumed to be in the Y-Z plane at an angle α to the Z axis, while θ is the equilibrium angle between Z and the film's magnetization. Since the X and Y axes are the easy axes of the in-plane biaxial anisotropy, the magnetization vector is confined to the Y-Z plane as well. The magnetization equilibrium condition reads

$$H_0 \sin(\theta - \alpha) - (H_d + H_a)\sin\theta\cos\theta - H_\parallel \sin^3\theta\cos\theta + H_\perp \sin\theta\cos^3\theta = 0. \quad \text{(A5)}$$

After solving it for the angle θ, we calculate the precession frequency using (A2) with a and b given by

$$a = H_0 \cos(\theta - \alpha) - (H_d + H_a)\cos 2\theta - H_\parallel \sin^2\theta\cos 2\theta + H_\perp \cos^2\theta\cos 2\theta, \quad \text{(A6)}$$

$$b = H_0 \cos(\theta - \alpha) - (H_d + H_a)\cos^2\theta + H_\parallel \sin^4\theta + H_\perp \cos^4\theta. \tag{A7}$$

Next, we calculate the precession frequency with an out-of-plane applied field when the in-plane tetragonal anisotropy is negligible ($H_\parallel = 0$) and the uniaxial in-plane field is along the Y axis. These assumptions apply well to the out-of-plane measurement on LCMO/NGO, Fig. 3(b), where we find $H_\parallel \approx 0$ and the applied field is in the Y-Z plane at angle α to the Z axis. The equilibrium position of magnetization is in the Y-Z plane with angle θ between Z and the magnetization vector. We can rewrite the magnetic free energy as

$$E = -\boldsymbol{H}_0 \cdot \boldsymbol{M} + 2\pi M_z^2 + K_a M_z^2/M_s^2 - K_u M_y^2/M_s^2 - K_\perp M_z^4/2M_s^4, \tag{A8}$$

and the equilibrium condition becomes

$$H_0 \sin(\theta - \alpha) - (H_d + H_a + H_u)\sin\theta\cos\theta + H_\perp \sin\theta\cos^3\theta = 0. \tag{A9}$$

The expressions for a and b are modified to be

$$a = H_0 \cos(\theta - \alpha) - (H_d + H_a + H_u)\cos 2\theta + H_\perp \cos^2\theta \cos 2\theta, \tag{A10}$$

$$b = H_0 \cos(\theta - \alpha) - (H_d + H_a)\cos^2\theta + H_u \sin^2\theta + H_\perp \cos^4\theta. \tag{A11}$$

Using (A2), (A10), and (A11) we calculate the precession frequency in the out-of-plane measurement on LCMO/NGO.

*Present address: Los Alamos National Laboratory, Los Alamos, NM 87545, USA. Electronic address: diyar@lanl.gov

[1] J.-H. Park, E. Vescovo, H.-J. Kim, C. Kwon, R. Ramesh, and T. Venkatesan, Nature (London) **392**, 794 (1998).

[2] Moon-Ho Jo, N. D. Mathur, J. E. Evetts, and M. G. Blamire, Appl. Phys. Lett. **77**, 3803 (2000).

[3] M. Bowen, M. Bibes, A. Barthélémy, J. -P. Contour, A. Anana, Y. Lemaitre, and A. Fert, Appl. Phys. Lett. **82**, 233 (2003).

[4] V. Garcia, M. Bibes, A. Barthélémy, M. Bowen, E. Jacquet, J.-P. Contour, and A. Fert, Phys. Rev. B **69**, 052403 (2004).

[5] V. Dedui, M. Murgia, F. C. Matacotta, C. Taliani, and S. Barbanera, Solid State Commun. **122**, 181 (2002).

[6] T. Ono, A. Kogusu, S. Morimoto, S. Nasu, A. Masuno, T. Terashima, and M. Takano, Appl. Phys. Lett. **84**, 2370 (2004).

[7] V. Dyakonov, V. Shapovalov, E. Zubov, P. Aleshkevych, A. Klimov, V. Varyukhin, V. Pashchenko, V. Kamenev, V. Mikhailov, K. Dyakonov, V. Popov, S. J. Lewandowski, M. Berkowski, R. Zuberek, A. Szewczyk, and H. Szymczak, J. Appl. Phys. **93**, 2100 (2003).

[8] R. Shreekala, M. Rajeswari, S. P. Pai, S. E. Lofland, V. Smolyaninova, K. Ghosh, S. B. Ogale, S. M. Bhagat, M. J. Downes, R. L. Greene, R. Ramesh, and T. Venkatesan, Appl. Phys. Lett. **74**, 2857 (1999).

[9] D. L. Lyfar, S. M. Ryabchenko, V. N. Krivoruchko, S. I. Khartsev, and A. M. Grishin, Phys. Rev. B **69**, 100409(R) (2004).

[10] S. E. Lofland, S. M. Bhagat, H. L. Ju, G. C. Xiong, T. Venkatesan, and R. L. Greene, Phys. Rev. B **52**, 15058 (1995).

[11] S. E. Lofland, S. M. Bhagat, C. Kwon, M. C. Robson, R. P. Sharma, R. Ramesh, and T. Venkatesan, Phys. Lett. A **209**, 246 (1995).

[12] A. I. Shames, E. Rozenberg, G. Gorodetsky, A. A. Arsenov, D. A. Shulyatev, Ya. M. Mukovskii, A. Gedanken, and G. Pang, J. Appl. Phys. **91**, 7929 (2002).

[13] Y. G. Zhao, J. J. Li, R. Shreekala, H. D. Drew, C. L. Chen, W. L. Cao, C. H. Lee, M. Rajeswari, S. B. Ogale, R. Ramesh, G. Baskaran, and T. Venkatesan, Phys. Rev. Lett. **81**, 1310 (1998).

[14] K. Matsuda, A. Machida, Y. Moritomo, and A. Nakamura, Phys. Rev. B **58**, R4203 (1998).

[15] A. I. Lobad, R. D. Averitt, C. Kwon, and A. J. Taylor, Appl. Phys. Lett. **77**, 4025 (2000).

[16] A. I. Lobad, R. D. Averitt, and A. J. Taylor, Phys. Rev. B **63**, 060410(R) (2001).

[17] R. D. Averitt, A. I. Lobad, C. Kwon, S. A. Trugman, V. K. Thorsmølle, and A. J. Taylor, Phys. Rev. Lett. **87**, 017401 (2001).

[18] Y. H. Ren, H. B. Zhao, G. Lüpke, Y. F. Hu, and Qi Li, J. Appl. Phys. **91**, 7514 (2002).

[19] T. Ogasawara, M. Matsubara, Y. Tomioka, M. Kuwata-Gonokami, H. Okamoto, and Y. Tokura, Phys. Rev. B **68**, 180407(R) (2003).

[20] S. A. McGill, R. I. Miller, O. N. Torrens, A. Mamchik, I. Wei Chen, and J. M. Kikkawa, Phys. Rev. Lett. **93**, 047402 (2004).

[21] S. A. McGill, R. I. Miller, O. N. Torrens, A. Mamchik, I. Wei Chen, and J. M. Kikkawa, Phys. Rev. B **71**, 075117 (2005).

[22] G. Ju, A. V. Nurmikko, R. F. C. Farrow, R. F. Marks, M. J. Carey, and B. A. Gurney, Phys. Rev. Lett. **82**, 3705 (1999).

[23] B. Koopmans, M. van Kampen, J. T. Kohlhepp, and W. J. M. de Jonge, Phys. Rev. Lett. **85**, 844 (2000).

[24] M. van Kampen, C. Jozsa, J. T. Kohlhepp, P. LeClair, L. Lagae, W. J. M. de Jonge, and B. Koopmans, Phys. Rev. Lett. **88**, 227201 (2002).

[25] Q. Zhang, A. V. Nurmikko, A. Anguelouch, G. Xiao, and A. Gupta, Phys. Rev. Lett. **89**, 177402 (2002).

[26] H. B. Zhao, D. Talbayev, Q. G. Yang, G. Lüpke, A. T. Hanbicki, C. H. Li, O. M. J. van 't Erve, G. Kioseoglou, and B. T. Jonker, Appl. Phys. Lett. **86**, 152512 (2005).

[27] Y. Suzuki, H. Y. Hwang, S.-W. Cheong, and R. B. van Dover, Appl. Phys. Lett. **71**, 140 (1997).

[28] K. Steenbeck and R. Hiergeist, Appl. Phys. Lett. **75**, 1778 (1999).

[29] J. O'Donnel, M. S. Rzhowski, J. N. Eckstein, and I. Bozovic, Appl. Phys. Lett. **72**, 1775 (1998).

[30] L. Ranno, A. Llobet, R. Tiron, and E. Favre-Nicolin, Appl. Surf. Sci. **188**, 170 (2002).

[31] C. M. Xiong, J. R. Sun, and B. G. Shen, Solid State Commun. **134**, 465 (2005).

[32] C. Kwon, M. C. Robson, J. Y. Gu, S. E. Lofland, S. M. Bhagat, Z.

Trajanovic, M. Rajeswari, T. Venkatesan, A. R. Kratz, R. D. Gomez, and R. Ramesh, J. Magn. Magn. Mater. **172**, 229 (1997).

[33] H. S. Wang, Q. Li, K. Lui, and C. L. Chien, Appl. Phys. Lett. **74**, 2212 (1999).

[34] H. S. Wang and Qi Li, Appl. Phys. Lett. **73**, 2360 (1998).

[35] H. S. Wang, E. Wertz, Y. F. Hu, and Qi Li, J. Appl. Phys. **87**, 7409 (2000).

[36] D. Talbayev, H. Zhao, G. Lüpke, J. Chen, and Qi Li, Appl. Phys. Lett. **86**, 182501 (2005).

[37] B. Vengalis, A. Maneikis, F. Anisimovas, R. Butkute, L. Dapkus, and A. Kindurys, J. Magn. Magn. Mater. **211**, 35 (2000).

[38] S. Zoll, H. A. M. Van den Berg, K. Ounadjela, D. Stoeffler, and A. Dinia, J. Appl. Phys. **79**, 2601 (1996).

[39] N. D. Mathur, M.-H. Jo, J. E. Evetts, and M. G. Blamire, J. Appl. Phys. **89**, 3388 (2001).

[40] M. Sasaura, S. Miyazawa, and M. Mukaida, J. Appl. Phys. **68**, 3643 (1990).

[41] M. L. Sanjuán, V. M. Orera, R. I. Merino, and J. Blasco, J. Phys.: Condens. Matter **10**, 11687 (1998).